

Comprehensive Glaucoma Imaging

Yoav Glidai, Malik Y. Kahook, Robert J. Noecker, Gadi Wollstein, and Joel S. Schuman

Contents

Introduction	2
Fundus Photography	3
General	3
Glaucoma Diagnosis and Monitoring	3
Advances in Fundus Photography	4
Optical Coherence Tomography	4
General	4
Glaucoma Diagnosis	5
Disease Progression Monitoring	10
Optical Coherence Tomography Angiography	12
Advancements in OCT Technology	14
Confocal Scanning Laser Ophthalmoscopy	16
Conclusion	16
References	17

Abstract

Advancements in ocular imaging over the past four decades have revolutionized glaucoma practice worldwide. As glaucomatous vision loss cannot be restored, early diagnosis, proper management, and timely intervention are essential to slow disease progression. The emergence of advanced computerized imaging modalities has shifted glaucoma assessment from being largely subjective to mostly objective. These modalities can document and accurately quantify the optic nerve head and the macula regions, which are affected by the disease. With various ocular imaging devices

Y. Glidai · G. Wollstein · J. S. Schuman (✉)
Department of Ophthalmology, NYU Langone Health,
New York, NY, USA
e-mail: gadi.wollstein@nyulangone.org;
schumanjs@gmail.com

M. Y. Kahook
Department of Ophthalmology, University of Colorado
School of Medicine, Aurora, CO, USA
e-mail: malik.kahook@gmail.com

R. J. Noecker
Ophthalmic Consultants of Connecticut, Fairfield,
CT, USA
e-mail: noeckerj@gmail.com

evolving over the years, optical coherence tomography (OCT) has become the dominant imaging technology in glaucoma practice. From the first prototype device to the newest swept-source OCT, each generation improved in image acquisition time, scan resolution, and artifact reduction, making structural assessment more accurate and sensitive. This advancement allows clinicians earlier detection of glaucoma diagnosis and increased sensitivity in monitoring of progression enabling timely modification of treatment to halt further damage. Moreover, the introduction of OCT angiography (OCTA) drew attention to the vascular component as an important element in glaucoma pathogenesis. In addition to technical advancements, the imaging field continues to evolve by the incorporation of innovative software such as image processing and artificial intelligence. Taken together, the role of ocular imaging is expected to further expand with a substantial impact on clinical management.

Keywords

Glaucoma · Imaging · OCT · OCTA · RNFL · ONH

Introduction

Helmholtz first described the visualization of the optic nerve head (ONH) in 1851 using the direct ophthalmoscope [1]. Only a few years later, Von Graefe described the optic atrophy seen in glaucoma as “amaurosis with excavation of the optic nerve” (amaurosis was a term used for “severe vision loss with a normal eye appearance”) [2]. The first pathologic description of glaucomatous ONH changes is credited to Schnabel, who noted that damaged nerve fibers accompanied this type of ONH damage [3]. Later on, in the 1920s, Fuchs and Elliot provided a detailed description of the glaucomatous changes. Fuchs described the progressive loss of the anterior glial fibers, followed by the posterior glial fibers with associated bowing backward and thinning of the lamina cribrosa

due to elevated intraocular pressure. Fuchs believed that these changes were significant and preceded visual field loss [4]. Fuchs’ assertions were subsequently supported by Quigley’s studies on glaucomatous cadaver eyes, showing that significant nerve fiber layer (NFL) loss occurs prior to detection of glaucomatous visual field defects [5, 6].

Studied extensively for decades, the relationship between glaucomatous structural changes and functional vision loss has been shown to be complex [7]. While the association between structure and function improves as the disease progresses (until reaching advanced disease with a reduced level of association), the relationship is difficult to define, especially in early glaucoma. Advancements in ocular imaging over the past four decades have allowed improved visualization and quantification of the typical glaucomatous findings. Utilizing these technologies, numerous studies have confirmed that structural damage often precedes the detection of vision changes with current functional testing technologies [8–11], increasing the clinical utility of imaging in glaucoma. As early detection and intervention can significantly alter the course of the disease by slowing neuronal damage and preventing vision loss, imaging became fundamentally essential in current glaucoma practice [12]. From the “Optic Nerve Head Analyzer,” generating measurements such as cup-to-disc (C:D) ratio and neuroretinal rim (NRR) area, to NFL thickness and vascular changes detected by the newest optical coherence tomography (OCT) and OCT angiography (OCTA) devices, each technology added sophistication to improve diagnosing, monitoring, and understanding glaucoma.

Glaucoma diagnosis depends on the clinician’s skills of detecting ONH damage, along with the characteristic visual field loss. The main ONH and NFL findings in glaucomatous eyes are increased C:D ratio, thinning or notching of the NRR, nasalization of the central retinal vessel trunk, vascular irregularity, disc hemorrhages, NFL defects, and peripapillary chorioretinal atrophy [13]. Evaluation of the ONH has been traditionally achieved through *subjective* methods, such as funduscopy examination and ONH photographs, though

accurate and reproducible methods are desired for diagnosis and monitoring. The subjective nature of ONH evaluation has led to a significant number of patients being undetected or being followed only as glaucoma suspects while others being suboptimally treated during times of disease progression [14]. These considerations have been the impetus to develop new technologies that can objectively and reproducibly evaluate the ONH and NFL.

With the aid of modern imaging techniques, clinicians are now afforded additional tools with which to assess and monitor their patients. These technologies have met the challenge of making ONH and NFL assessment more sensitive, accurate, and reproducible while becoming more reasonably priced, user-friendly, and practical for office use. While imaging modules are gaining growing clinical acceptance, one must remember that they are only one assessment tool that accompanies clinical examination, history taking, and functional visual testing. Imaging devices are essential to, but cannot replace, clinical assessment and integrative decision-making.

This chapter will summarize the important developments in imaging of the ONH and NFL using fundus photography, Heidelberg retinal tomography (HRT), and optical coherence tomography (OCT). Each section will describe the technology and its role in glaucoma diagnosis and monitoring.

Fundus Photography

General

The first retinal photographs of a living human subject were published in 1886 by Jackman and Webster, whose camera was mounted on the patient's head and had a two and a half minutes exposure time [15]. The main obstacle with those early images was a prominent corneal reflex, which was later overcome by Dr. Walter Thorner and Dr. Dimmer, who used the same principles of the indirect ophthalmoscope [16]. In 1925, Dr. Nordenson of Stockholm, who worked with the Zeiss company, produced the Zeiss-Nordenson

camera, which became a widely used fundus camera [17]. During the subsequent few decades, capturing retinal photographs gained popularity, and the technology evolved to permit the use of color film, electronic flash, better optics, and an affordable price to ophthalmology practices around the world [17].

Glaucoma Diagnosis and Monitoring

Fundus cameras have been used to monitor and diagnose glaucoma for decades [18]. Several photographic techniques have been utilized for that purpose. Stereoscopic photography was performed using nonsimultaneous exposures with lateral shifts of the fundus camera or the Allen separator that creates a more consistent stereo base, giving the appearance of a three-dimensional image. Another technique is red-free photography, which highlights the nerve fibers brightness and texture, assisting in the recognition of NFL defects. Although fundus photography produces an objective image of the ONH, its interpretation still involves subjectivity, which in turn increases variability and limits its usefulness in the long-term evaluation of glaucoma patients [19, 20]. It has been shown that other imaging technologies (i.e., HRT and OCT) outperform most observers in the diagnostic accuracy of optic disc photographs [21]. An extensive review showed that the pooled sensitivity for identifying glaucoma using disc photography was 73% and 75% (using C:D ratio or NFL defects, respectively) and specificity of 89% and 88%, respectively [22].

Strengths

1. Document accurately clinical findings for future follow-up
2. Higher sensitivity in detecting disc hemorrhages than clinical examination [23]

Weaknesses

1. Interpretation of photographs is subjective
2. Reduced image quality with small pupils or media opacities

Advances in Fundus Photography

The traditional fundus camera systems were table-mounted and bulky, comprised of complex optical and mechanical components. Those were very large in size, high in costs, and needed a trained technician to operate. The introduction of portable cameras and smartphone-based fundus imaging systems has resulted in an exponential surge in available technologies for portable fundus photography. Inexpensive, mobile, and easy-to-operate cameras can revolutionize retinal screening programs around the world, especially in areas with limited access to ophthalmologists through the use of telemedicine [24, 25].

Another emerging advancement in the field is the automated fundus photography analysis using artificial intelligence (AI). Designing a computer-based assessment for glaucoma still poses a challenge due to the highly variable and complex appearance of the ONH. Furthermore, applying a reliable machine learning classifiers to color fundus photographs requires a large number of examples to train AI algorithms [26]. Nonetheless, recent machine learning studies, which processed more than hundreds of thousands of fundus photographs, reported a robust performance with an area under the receiver operating characteristic curve (AUC) of over 0.94 for identifying discs worthy of referral for specialized care [27, 28]. While it appears to be promising, this technology requires dilated pupils, has reduced portability, and relies on skilled technicians, limiting its role as a glaucoma-screening device [25].

Optical Coherence Tomography

General

Optical coherence tomography (OCT) is a non-invasive, non-contact imaging technology that produces high-resolution cross-sectional images of the retina that was first introduced in 1991 [29]. The light source used is from a near-infrared, low-coherence superluminescent diode at a wavelength of 810 nm or 1030 nm. The exiting light is split into two arms with one beam entering the

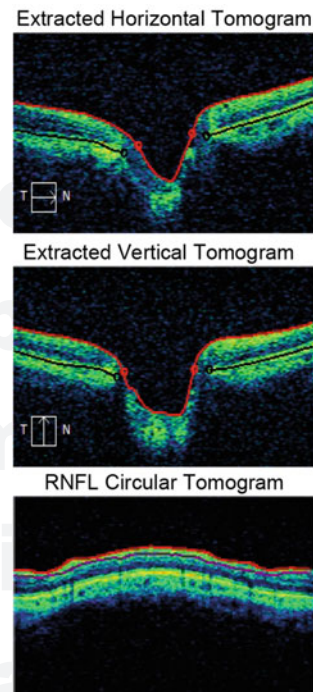


Fig. 1 False color B-scans of a healthy optic nerve head and peripapillary area

eye, and the other sent to a reference mirror. If the path length of the two arms is closely matched to within the coherence length, an interference signal is detected and translated into a two-dimensional color-coded representation of the retinal layers. Cross-sectional two-dimensional images (B-scans) are generated by performing multiple, adjacent axial measurements (Axial scans, or A-scans) and scanning the incident optical beam transversely. These B-scans can be displayed in false color or grayscale (Fig. 1). Three-dimensional, volumetric data sets can be generated by scanning the incident optical beam in a raster pattern using sequential cross-sectional scans.

OCT imaging devices became commercially available in 1996, with the first generation implementing a technique referred to as timedomain OCT (TD-OCT). TD-OCT encodes the reflection location in the time information, relating the location of the reflection to the position of a moving reference mirror. The primary commercially available TD-OCT device was the Stratus OCT™ made by Zeiss. Although scans

of the TD-OCT could discriminate a glaucomatous eye from a healthy eye [30–32] and detect change over time [9, 33], the technology was restricted by slow acquisition times that limit the ability to acquire dense sampling of an area such as the macula or the ONH regions [34].

Spectraldomain (SD-OCT) (the most common commercial device at the time of this writing) employs a Fourier domain transformation method. While TD-OCT scanned in a speed of 400 A-scans/sec with an axial resolution of 10 μm , SD-OCT scans at a speed of 27,000 A-scans/sec with up to 3–6 μm axial resolution [35]. These advancements are leading to improved measurement reproducibility and accuracy in identifying glaucomatous eyes, decreased artifacts, and reduced scan acquisition time [35–40]. Being that the human eye moves very fast and involuntary, improvement in acquisition speed means fewer motion artifacts [41]. SD-OCT acquires all information within a single axial scan simultaneously through the tissue by evaluating the frequency spectrum of the interference between a stationary reference mirror (rather than moving, in TD-OCT) and reflected light. Several manufacturers are producing the SD-OCT system.

Swept-source OCT (SS-OCT) is another form of Fourier domain OCT that utilizes a single tunable laser that sweeps through different frequencies to rapidly cover the entire broad spectrum [42]. The reflectance of the light from the retina is captured by a photodetector that is much faster than the charge-coupled device camera used in SD-OCT [43]. This technology allows a faster scanning speed of up to 400,000 axial scans/second, improving scan quality further, and reducing distortions caused by eye movements. Moreover, most SS-OCT systems use a longer wavelength laser of approximately 1030 nm, resulting in greater tissue penetration, allowing better visualization of deeper ocular structures like the choroid, sclera, and lamina cribrosa [44]. As of the writing time of this chapter, two SS-OCT platforms are approved for use in the USA.

In recent years, OCT technology has changed the paradigm of retinal assessment and revolutionized the management and diagnosis of glaucoma. As OCT provides high-resolution visualization of

ocular microstructures and the ability to objectively and precisely evaluate the retinal nerve fiber layer (RNFL), macula, and the ONH, it has established itself as the dominant imaging modality in the practice of glaucoma [34, 45].

Glaucoma Diagnosis

The most commonly used OCT parameter for glaucoma diagnosis and monitoring is the RNFL thickness that provides an indicator of the damage to the ganglion cell axons. RNFL thickness is assessed in the peripapillary region where axons from the entire retina gather to form the optic nerve. This information can be displayed as a thickness map of the peripapillary area or as the thickness profile in a circle of 3.4 mm diameter centered on the ONH (Fig. 2). ONH reports from most OCT devices provide thickness maps, and various RNFL and ONH parameters with both eyes side by side for comparison can be displayed on most OCT reports (Fig. 3). The report usually includes numerous maps: the RNFL thickness map (Fig. 3a), and its deviation from age-matched healthy population (Fig. 3c), horizontal and vertical crosssections, and a circular crosssection (Fig. 3c) along the ONH's centered purple circle appearing in Fig. 3b. RNFL thickness profile along this circle (Fig. 3d), in quadrants and 12 clock-hours (Fig. 3e), are also provided along with a neuroretinal rim thickness profile map (Fig. 3f). In addition to these maps, quantitative information is provided for key ONH and RNFL

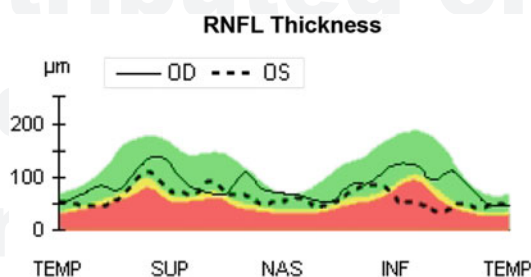


Fig. 2 Cirrus circumpapillary RNFL thickness profile map of a 53-year-old woman with glaucoma, showing decreased RNFL thickness in OS, especially in the inferior quadrant

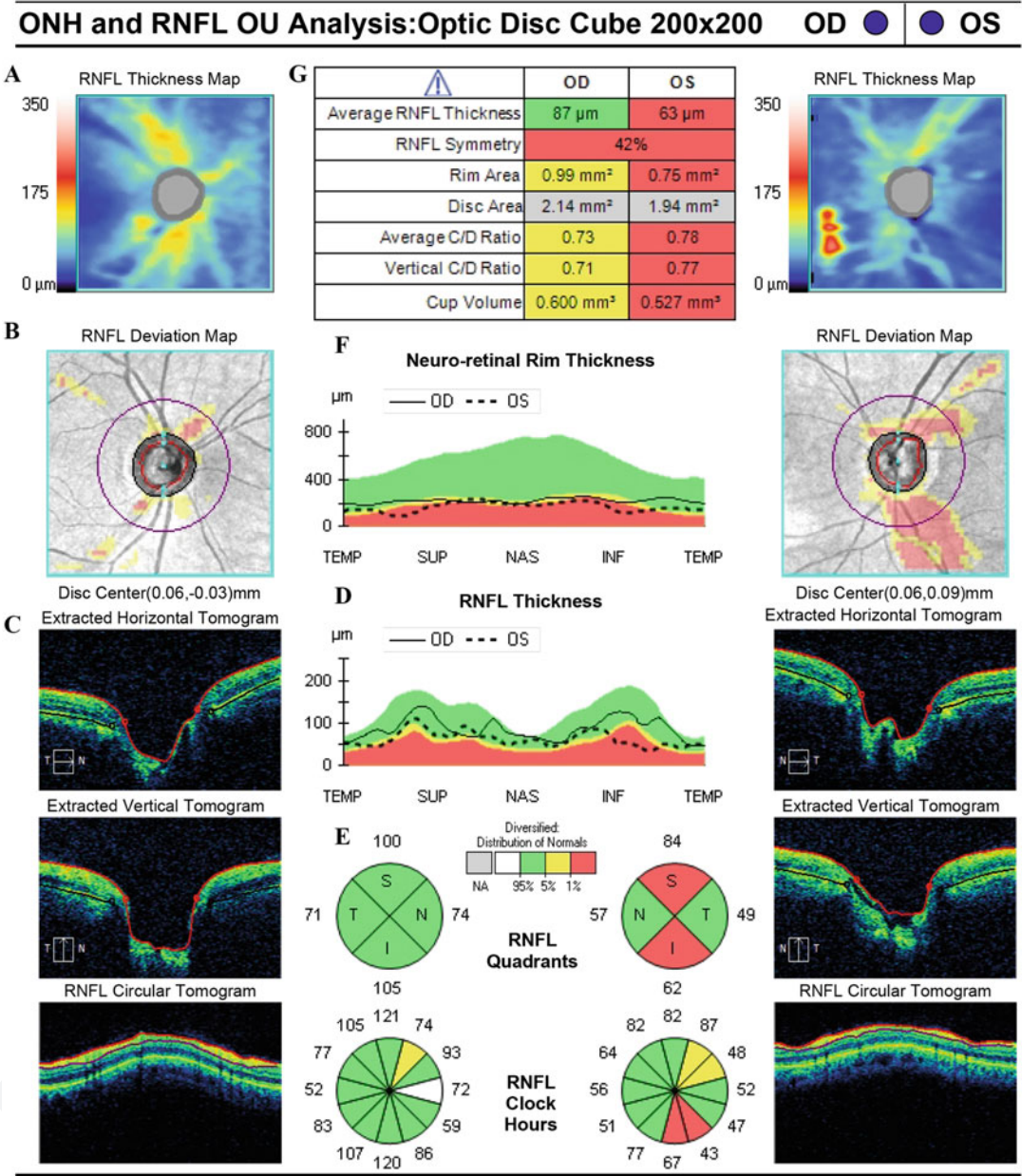


Fig. 3 Cirrus ONH and RNFL OU analysis. A 53-year-old woman with glaucoma. The report contains (a) RNFL thickness and (b) deviation maps that facilitate the detection of localized damage. (c) Linear and circular cross section overlaid with layer segmentation. (d) Circumpapillary RNFL thickness profile and (e) RNFL

thickness measurements in quadrants and clock hours showing damage in OS. (f) Neuroretinal rim thickness profile. (g) Key ONH and RNFL parameters, showing increased C/D ratio in both eyes, more pronounced in OS. Average RNFL thickness is normal OD but reduced OS

parameters (Fig. 3g). Reported parameters are compared to a normative database and color-coded in yellow or red if the value is identified

in less than 5% or 1% of the normative database population, respectively. The RNFL deviation map (Fig. 3b) shows areas in which RNFL

thickness is lower than 5% and 1% of the normative database.

The RNFL parameters most often used by clinicians for glaucoma diagnosis are average (global) RNFL thickness and inferior and superior quadrants RNFL thickness [34, 46, 47], which is in agreement with the known superior and inferior RNFL damage in early glaucoma. For detection of glaucoma, SD-OCT RNFL parameters achieved sensitivities ranging from 60% to 98% and specificities ranging from 80% to 95%, with an AUC >0.9 [34, 48]. Whereas diagnostic performance improves as the disease progresses, detecting early glaucoma with minimal VF loss still poses a challenge, as SD-OCT have reduced sensitivity in early cases [49, 50]. Nonetheless, it is essential to follow and image those glaucoma suspects, as it was shown that RNFL changes could be evident up to 8 years before the appearance of VF defects [8].

Unattainable by previous nerve fiber analysis devices, OCT can provide detailed information about the macula. Macular damage occurs early in the course of the disease and can present as arcuate defects, diffuse damage, local damage, or any combination of those. With the development of improved segmentation algorithms, macular parameters have been suggested as an alternative or as a complementary analysis to peripapillary RNFL thickness. Compared to the ONH region, the macula is an area of less variability and has a lower probability of having an abnormal structure; hence it would generate measurements that are less affected by anatomical variability. Moreover, retinal ganglion cells (RGC) have a larger diameter than their axons (RNFL), and the macular RGC layer is up to seven cells thick, containing the majority of the eye's RGC [51], making it an area sensitive to glaucomatous RGC damage.

The most common OCT macular parameters in use are the ganglion cell and inner plexiform layer (GCIPL) thickness and the ganglion cell complex (GCC; includes macular RNFL and GCIPL) thickness. Macular thickness measurements can distinguish glaucomatous from healthy eyes and correspond well with the location of VF defects [52–54]. The macular OCT report includes thickness (Fig. 4a) and deviation (Fig. 4b) maps of the

GCIPL of both eyes. Sectoral GCIPL thickness (Fig. 4c) and summary table (Fig. 4d) are provided, with the deviations of the GCL+IPL thickness being color-coded, differentiating between deviations appearing in less than 5% and 1% of database population. In the present subject (Fig. 4), extensive glaucomatous damage is present in OS. Linear crosssections with layer segmentation are also provided (Fig. 4e). A recent meta-analysis concluded that average macular parameters were similar or slightly inferior to average peripapillary RNFL [47]. Although macular evaluation showed comparable performance and exhibits a promising alternative, it seems that peripapillary RNFL remains the most diagnostically accurate OCT analysis for detecting glaucoma.

The ONH parameters most commonly used and with the best diagnostic ability are (1) vertical cup-to-disc ratio (2) rim area and (3) rim volume [55]. A relatively new anatomical ONH parameter is Bruch's membrane opening minimal rim width (BMO-MRW), corresponding to the minimal distance between the BMO and the internal limiting membrane. BRO-MRW correlates well with VF functional decline and shows a similar ability to detect glaucomatous eyes compared with RNFL and ONH parameters [56, 57].

It has been well established that most ONH parameters have a good discriminate ability between healthy and glaucomatous eyes. When comparing ONH versus RNFL or macular parameters, there are conflicting reports regarding diagnostic superiority. Several studies have shown a similar or even better diagnostic ability for ONH parameters, while others concluded that RNFL and macular parameters are significantly better [34, 38, 46, 56, 58].

One of the new features of SS-OCT systems is their ability to capture a wider scanning area (9×12 mm), including both the macula and ONH areas in one scan. The generated report includes circumpapillary RNFL B-scan (Fig. 5a); circumpapillary RNFL thickness map with color-coded probability information relative to healthy subjects, with a dashed line showing the borders of the quadrants and red lines showing the average locations of the major vessels (Fig. 5b); sectoral RNFL thickness measurements in quadrants and

Ganglion Cell OU Analysis: Macular Cube 200x200

OD OS

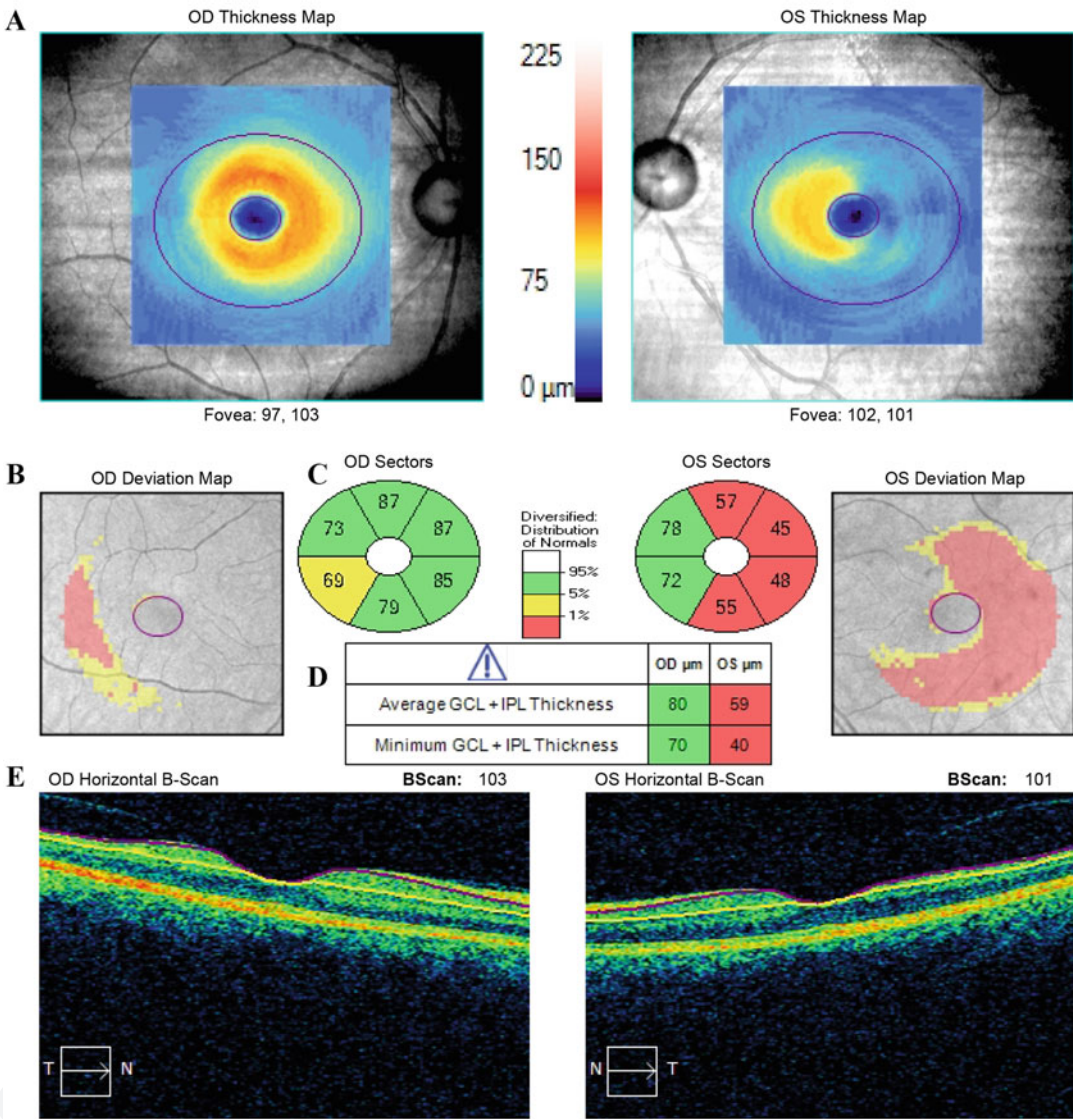


Fig. 4 Cirrus macular report of ganglion cell layer of a 53-year-old woman with glaucoma (same subject presented in Fig. 3). Ganglion cell and inner plexiform layer (GCIPL)

thickness is reduced OS in the inferior, temporal, and superior regions

clock hours with color-coded probability (Fig. 5c); en face image with a thickness heat map (Fig. 5d); associated probability map for the RNFL thickness map aligned based upon the centers of the disc and macula; and RGC thickness map with probability map (Fig. 5e, f). Additionally, it is possible to superimpose visual field tests on the RNFL and macular map for structure-function relationship

interpretation (Fig. 5e, f). This one-page report was shown to be very helpful in discriminating healthy and glaucomatous eyes when used by a non-glaucoma specialist [59]. Furthermore, SS-OCT single widefield scan was able to distinguish between pre-perimetric and early perimetric glaucoma patients from healthy controls and to detect progression successfully [60–62].

This document is copyright of the original publisher. This document is strictly private, confidential and personal to its recipients and should not be copied, distributed or reproduced in whole or in part, nor passed to any third party.

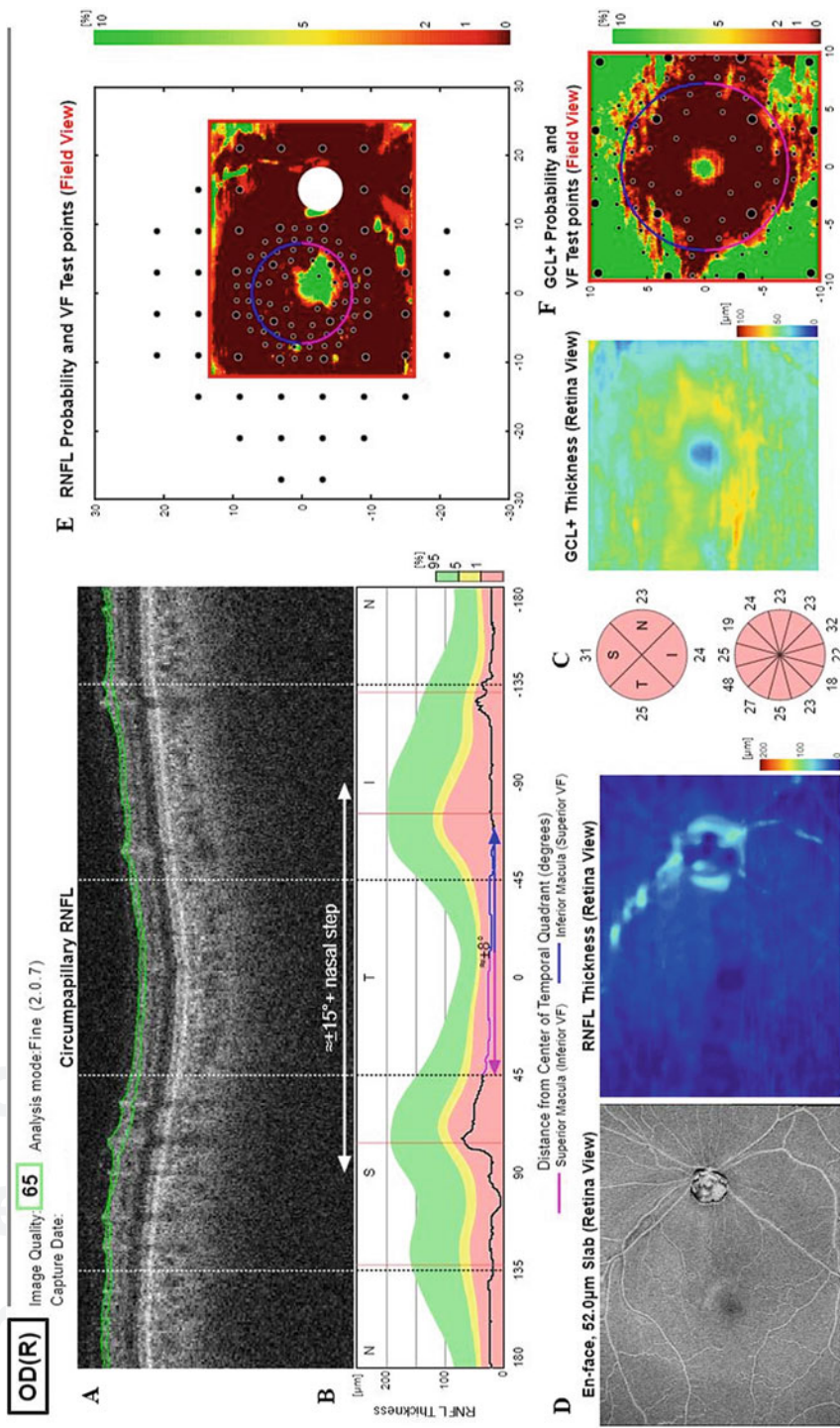


Fig. 5 A single page report based on wide field SS-OCT scan, showing RNFL, macular, and visual field analysis. (Courtesy of Fabio Lavinsky, MD)

Albeit some OCT parameters have been shown to detect glaucoma better than others, it is recommended to consider a combination of parameters in the diagnostic process. Diagnosis of glaucoma is often challenging, and patients usually have some structural variability that can influence the measured parameters. A proper combination of peripapillary RNFL, ONH, and macular parameters will further improve diagnostic performance. One of the most promising approaches for handling multiple parameters is automated machine learning methods that gained large popularity. These methods, and more specifically, the deep learning method, show encouraging results for diagnosis and prediction of disease progression [63, 64].

Disease Progression Monitoring

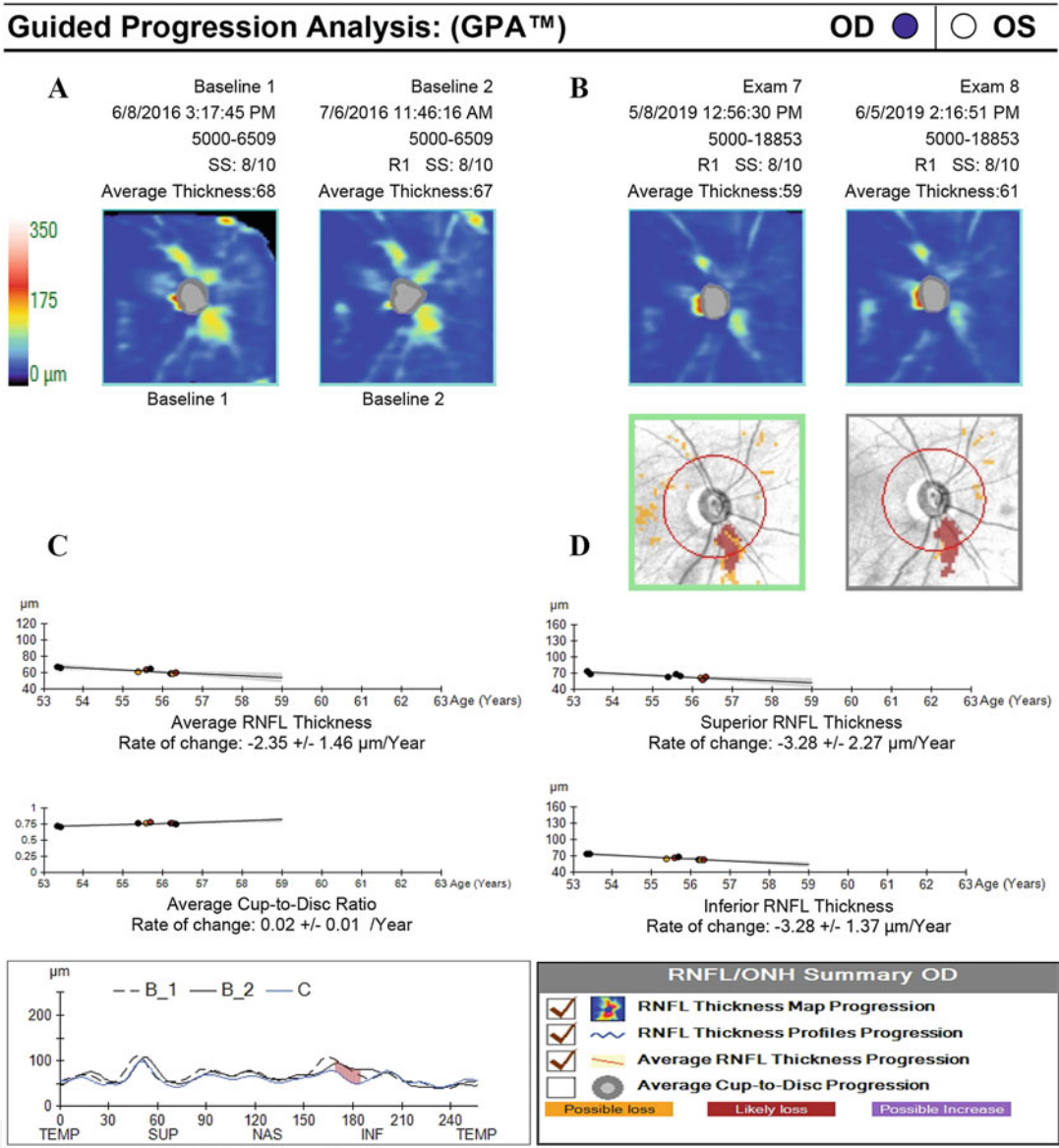
Using a prototype TD-OCT, the first longitudinal study to evaluate glaucoma progression with peripapillary RNFL parameters demonstrated the potential of OCT in detecting longitudinal change better than VF testing [9]. Whereas TD-OCT devices were limited by inferior reproducibility and slower scanning speed, the improved capabilities of SD-OCT also allow registration of sequential scans, which are all translated to improved sensitivity to detect disease progression. Most SD-OCT platforms have a progression analysis program (i. e., guided progression analysis, or GPA, in Cirrus devices, Fig. 6) that can assess progression by either event-based or trend-based analysis. The event-based analysis identifies disease progression when a follow-up measurement exceeds a pre-established threshold. In contrast, trend-based analysis detects progression based on the slope of a measured parameter over time. Both analyses showed similar performance in detecting progression [65], although each approach has its limitations. The event-based analysis is limited by outliers that can be falsely identified as progression. The trend-based analysis is less sensitive to measurement variability, but it requires a large number of measurements to be considered reliable [48].

RNFL, macular, and ONH parameters have all been shown to change at a faster rate in glaucoma

progressors. For years studies were aimed to establish which parameter is most accurate in detecting progression, with a recent extensive review summarizing the data collected. The most common parameters used in studies were RNFL average thickness and macular parameters (either GCIPL or GCC) [66]. Due to different baseline thickness and dynamic ranges in various studies and parameters, a comparison can be made only by using normalized data. Using this approach, it was reported that normalized RNFL thickness decreases by 1.7% per year compared with only 1.3% per year in GCIPL (absolute means were $-0.98 \mu\text{m}/\text{year}$ vs. $-0.57 \mu\text{m}/\text{year}$) [67]. In eyes with advanced glaucoma, when no further decline in RNFL can be detected (known as the “floor effect”), a significant slope in GCIPL was observed [67]. Therefore, the diagnostic utility of these two parameters varies depending on the stage of the disease. In early to moderate disease, RNFL is more sensitive in detecting disease progression, whereas GCIPL is a better indicator in advanced disease when RNFL has reached its “floor effect” [66, 68].

Identifying subjects with glaucoma that are at a higher risk for rapid progression is a primary goal in practice as it will dictate treatment options and frequency of clinical visits, and therefore it is desirable to determine it as early as possible. In the Advanced Imaging for Glaucoma study, baseline borderline and abnormal GCC and RNFL parameters were significant predictors of future functional damage [69]. Subjects with abnormal baseline parameters had a five times increase in the likelihood of converting to a confirmed glaucomatous VF [69]. Of note, not all suspects who presented with abnormal baseline findings eventually progressed, so application in clinical practice should be made with caution.

Even when RNFL measurements are accurate, distinguishing between glaucomatous structural damage, measurement variability, and age-related structural loss remains a challenge [48]. In a longitudinal study, age-related average RNFL decline was shown to be $-0.52 \mu\text{m}$ per year for average RNFL and $-1.25 \mu\text{m}$ in the inferior quadrant thickness [70]. Additionally, subjects with higher baseline thickness showed a faster rate of



of 2.18 μm for RNFL and 1.39 μm for GCC); hence it will not have a substantial effect on progression detection over short-term follow-up. Nonetheless, over many visits or years of follow-up, the aging effect becomes significant and should be considered in the disease monitoring practice.

An additional factor to be considered when monitoring disease progression is measurement variability. SD-OCT was shown to have excellent repeatability for all parameters [36, 66]. Intra-visit variability (test-retest standard deviation) for average RNFL is 1.18 μm , and for quadrants range between 2.16 and 2.84 μm . Between visit variability for average RNFL is 1.67 μm , and quadrants ranged between 2.82 and 3.49 μm [72]. ONH and macular parameters measured by SD-OCT also showed excellent repeatability. Test-retest variability was reported to be 1.45 μm for average GCIPL thickness and between 1.54 to 2.16 μm for sectoral GCIPL thickness [73].

Based on the test-retest standard deviation presented, it was suggested that a short-term change in average RNFL thickness of more than 4–5 μm should raise suspicion for disease progression [36, 72]. Due to worst reproducibility of sectorial averages compared with the global average, only a more significant decline in sectoral RNFL thickness would indicate actual change (approx. 7 μm in the inferior, superior, and temporal quadrants or 8 μm in the nasal quadrant) [72].

Since the introduction of OCT more than two decades ago, our ability to detect and quantify glaucomatous structural changes has been greatly enhanced. OCT provides means to obtain reproducible measures of the RNFL, ONH, and macula, all essential in quantifying glaucoma progression. Subjects with progressive changes on OCT are at increased risk of developing VF defects and of having a faster decline in quality of life [66]. Proper and prompt detection of those changes will allow treatment escalation at an earlier point to better preserve vision and quality of life.

Strengths

1. Detailed cross-sectional imaging

2. Rapid and accurate RNFL, ONH, and macula visualization and measurements
3. High axial resolution
4. Progression analysis of ONH, RNFL, and macula parameters is available

Weaknesses

1. Media opacity might prevent reliable imaging

Optical Coherence Tomography Angiography

There is mounting evidence of the key role of vascular components in glaucoma pathogenesis. Nonetheless, it remains unclear what is the exact contribution of such factors and at what stage they have an impact. Optical coherence tomography angiography (OCTA) is a novel technology that allows three-dimensional, detailed imaging of retinal and choroidal blood vessels. OCTA is based on detecting differences in intensity, amplitude, or phase variance between sequential B-scans taken at the same location of the retina. A series of B-scans at the same transverse location is taken and registered to one another. The degree of de-correlation between scans, which originate from the moving component of the scan, is calculated. As a result of the erythrocytes movement, imaging of blood vessels is achieved [74]. In other words, OCTA creates “motion-contrast” images of the retinal vasculature. Over the recent years, OCTA has increased importance in the diagnosis and management of different retinal diseases as it provides detailed three-dimensional information of retinal and choroid vessels, previously acquired only by conventional angiography. Compared to conventional angiography, OCTA is non-invasive, avoiding the potential risks of intravenous dye injection [75, 76]. As to this writing, only two OCTA devices are commercially available in the USA, which are AngioPlex (Carl Zeiss, Dublin, CA, USA) and AngioVue (OptoVue, Fremont, CA, USA). Other platforms are presently available only outside the USA: Triton Swept Source OCT (Topcon, Japan), AngioScan (Nidek, Japan), the OCTA Module (Heidelberg, Germany), and the Canon Angio eXpert (Canon, Japan).

One of the biggest riddles regarding microvascular changes is whether these changes are the etiology or an outcome. Several OCTA studies attempted to answer that question, with meaningful but sometimes contradicting findings. Some investigators wish to deduce a timeline from multiple cross-sectional studies. However, only longitudinal studies with a large cohort would deliver precise evidence.

The OCTA report includes maps of the vasculature at different layers of retina and choroid (Fig. 7). An en face image portrays blood vessels as a bright signal, while dark areas represent no flow or flow too slow to detect. The vascular parameters included in the report are (1) vessel density (VD), (2) perfusion density, (3) flow index, and (4) foveal avascular zone (FAZ). VD is measured as the total number of pixels with perfused vasculature per area unit. Perfusion density is the total area of perfused vasculature per area unit.

Several studies showed that peripapillary VD of glaucomatous eyes is lower compared to healthy controls [77, 78]. It was since shown that OCTA parameters, both macular and peripapillary, can distinguish well between glaucomatous and healthy eyes, with comparable diagnostic performance to RNFL thickness [78–83]. In particular, average peripapillary VD is the most assessed parameter, showing good discriminating ability, with AUC ranging between 0.78 and 0.96 [84]. Furthermore, a recent study found that glaucoma suspects had a significantly higher inter-retina peripapillary and macular VD asymmetry compared to healthy eyes, suggesting that OCTA might be utilized for early detection of glaucoma [85]. Of note, the majority of studies found a significant decline in the superficial retinal layers, but not in the deep. This discrimination could reflect a different involvement of each plexus in

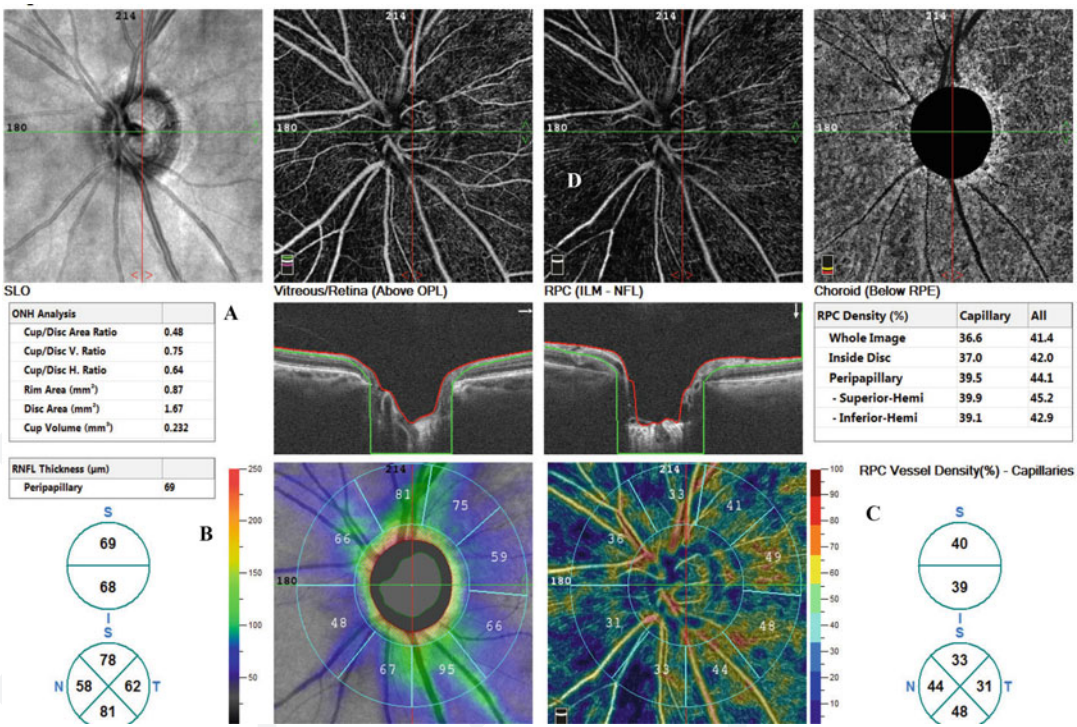


Fig. 7 OCTA report of a 74-year-old woman with glaucoma at a moderate stage. The report contains (a) ONH parameters, (b) peripapillary RNFL thickness map, divided into quadrants and hemifields, (c) radial

peripapillary capillary vasculature (RPC) analysis, showing VD measurements in quadrants and hemifields, and (d) en face slab angiography scans of various depths

the pathogenesis of glaucoma, or it could have been caused by a flow projection artifact [83].

OCTA parameters correlate well with VF function [77, 83, 86, 87]. Furthermore, several studies reported that all three networks showed stronger OCTA-function association compared to traditional OCT parameters [83, 88]. It was also demonstrated that pre-perimetric primary open-angle glaucoma (POAG) eyes had significantly lower mean VD than healthy eyes (52.0% vs. 55.9%, $p < 0.001$) [82]. Another study found that in perimetrically intact regions of glaucomatous eyes, mean VD, as well as RNFL thickness, were significantly reduced in some sectors compared with healthy controls [89]. These findings might suggest that vascular changes precede functional decline; however, the precise relationship between the markers appears to be complex. While both RNFL thinning and peripapillary VD decline seem to precede VF loss, they occur independently of each other in different retinal sectors [89, 90].

OCTA parameters of all areas have good intra-visit repeatability in subjects with glaucoma [83, 91]. As OCTA introduced only recently, at the time of this writing, there is no information about the ability of this device to track changes longitudinally. One possible promising application of vascular parameters in glaucoma practice could be monitoring beyond the “floor effect” of RNFL thickness measurement. Using a broken stick linear model, a cross-sectional study comparing the floor of perifoveal vessel density, circumpapillary capillary density, RNFL, and GCC thickness showed that perifoveal VD was the only marker that continued to decline consistently until very advanced disease [92].

Detection of glaucomatous damage in highly myopic eyes is challenging due to myopia-induced RNFL thinning [91]. However, peripapillary perfused capillary density (vessel density with large vessels removed) showed a progressive reduction in mean capillary density from healthy eyes to myopic eyes without glaucoma, glaucomatous eyes without myopia to glaucomatous eyes with myopia [93]. Another study showed that peripapillary VD have a better correlation with VF parameters than peripapillary

RNFL measurement in subjects with glaucoma and high myopia, where no significant correlation was detected in glaucomatous eyes without myopia [94]. These reports indicate that OCTA parameters might be useful in the diagnosis and monitoring of glaucoma in myopic eyes. Nevertheless, the cross-sectional nature of these studies cannot determine the causation between vessel density and glaucomatous damage.

Strengths

1. Discriminate between glaucomatous and healthy eyes
2. Might be useful for glaucoma diagnosis in myopic eyes

Weaknesses

1. Blood flow is detected within a specific range. Blood vessels with flow above or under this range will be undetected

Advancements in OCT Technology

Adaptive Optics

Adaptive optics (AO) is an image enhancement method that improves quality by removing optical aberration. Adopted from the astronomy discipline, AO was designed to remove atmospheric turbulence when imaging astrophysical objects from ground-based telescopes. To attain that enhancement, AO systems utilize a wavefront sensor to measure and correct optical aberrations in realtime, with an electro-actuated deformable mirror that alters the shape of the incoming wavefront to compensate for distortions [95]. When applied to the optical apparatus of the eye, AO provides substantial improvements in the sharpness of images that is typically impaired by ocular aberrations. While SD-OCT technology succeeded in reducing the axial resolution from 10 to 3–6 μm , the transverse resolution was still limited by the optical properties of the eye to a resolution of only 15–20 μm [42]. AO has substantially improved retinal image quality by reducing the transverse resolution to 2–5 μm and minimizing granular image artifacts and spackle size [95].

Since its introduction to ophthalmology in 1989 [96], AO was first implemented in fundus photography, subsequently gaining importance in other imaging modalities such as scanning laser ophthalmoscopy and OCT [97]. The incorporation of AO allows in vivo visualization of microscopic structures, such as photoreceptors, RNFL bundles, ganglion cells, and the lamina cribrosa (LC), thus expanding the horizon of ophthalmic research [98]. In glaucoma, as early diagnosis is a fundamental objective, increased ability to image subtle microscopic changes in the RNFL at the preclinical stage could be of immense value to early disease detection. Ganglion cells are the primary target of glaucomatous damage, and the ability to evaluate them in vivo might revolutionize glaucoma detection and monitoring [99]. Another area of particular interest is the LC that is a primary site for initial glaucomatous damage. AO allows visualization of the LC microstructure and macrostructure, permitting the in-depth characterization of those structures [100–103]. LC role in glaucoma is yet to be fully understood, though AO technology paired with the deeper penetrating SS-OCT does show great promise in the ongoing study of glaucoma pathogenesis.

Polarization-Sensitive OCT

Every tissue of the eye has distinct polarization properties that alter light when it passes through it. Polarization-sensitive OCT (PS-OCT) is a technology that allows differentiation between tissues based on the light-tissue interaction, adding another contrast channel and quantitative data to the image [42, 104]. A glaucoma model experiment of primates demonstrated that decreased RNFL reflectance was associated with glaucomatous damage, speculating that reduced reflectance stems from mitochondrial dysfunction or retinal ganglion cell death [105]. A new normalized reflectance index that incorporates reflectance input, as well as RNFL thickness, outperformed RNFL thickness alone in distinguishing human glaucoma suspects from healthy controls [106]. Another study showed a significant association between the reduction in the RNFL reflectance intensity ratio and the rate of VF deterioration [107].

Furthermore, changes in reflectance might precede RNFL thickness decline [108], suggesting that RNFL reflectance, as measured by PS-OCT, could be a promising candidate for early diagnosis of glaucoma [42, 84, 106].

OCT Doppler

In Doppler OCT, moving erythrocytes scatter the projected light, causing a shift in the optical frequency. The amount of shift is related to flow velocity, providing a non-contrast method to image and quantify retinal blood flow. While OCTA is designed to separate moving scatters from static background tissue in order to create angiograms [74], Doppler OCT uses the Doppler phase shift to *quantify* blood flow [109]. It has been demonstrated that subjects with hemifield VF defect exhibit reduced retinal blood flow in both the affected and the unaffected hemiretinas [110]. Furthermore, decreased blood flow was correlated with RNFL thinning [110]. As blood flow represents tissue function, OCT Doppler adds another layer to further understanding glaucoma pathogenesis.

Phase-Sensitive OCT (PS-OCT)

This technology analyzes the phase information of the back-reflected light beam, which is typically ignored in conventional OCT systems. The phase-sensitive OCT technique can provide in vivo information on micron-scale movements or vibrations within the tissue. A change in tissue structure that occurs as a result of applied stress can be quantified, providing information on tissue stiffness and elasticity, a technology referred to as optical coherence elastography (OCE). PS-OCT can be utilized to study the biomechanical properties of various ocular structures, including the cornea, lens, sclera, retina, trabecular meshwork, and optic nerve [111]. For example, precise information of corneal biomechanics obtained with PS-OCT can greatly assist early diagnosis and optimal management of corneal diseases such as keratoconus in addition to the evaluation of healthy corneas before refractive surgery [112, 113].

Vertical-Cavity Surface-Emitting Laser (VCSEL)

The vertical-cavity surface-emitting laser, or VCSEL, utilizes a semiconductor laser light source with the main advantage of providing a substantially deep scan. Using the VCSEL method, it is possible to image the entire globe, from the cornea to the optic nerve in a single scan, and create a three-dimensional reconstruction of the globe [114, 115]. The clinical utility of this device is still under investigation.

Confocal Scanning Laser Ophthalmoscopy

The Heidelberg Retinal Tomography (HRT; Heidelberg Engineering, Heidelberg, Germany) is a confocal scanning laser ophthalmoscope (CSLO) that provides quantitative measurements of the ONH and the posterior segment. This device was a primary clinical ophthalmic tool until a few years ago when it was sidelined by OCT. At the time of this writing, this device is no longer available for purchase from the manufacturer in the USA. As such, we will only briefly introduce this device.

The HRT projects a 670 nm wavelength light from a diode laser through a pinhole toward the posterior pole. Back-reflected light passes through a second, conjugated pinhole to a detector, ensuring that only light reflected from a defined focal plane will reach the detector. A set of 16–64 sequential two-dimensional scans are then reconstructed to form a three-dimensional data set of reflection intensities. A topographical map is created representing the location of maximal intensity of light at each pixel. The user needs to mark the optic nerve head margin to obtain quantitative measurements of the ONH. The primary use of the device was for ONH analysis, while the limited axial resolution restricted its use for macula examination.

HRT parameters were demonstrated to perform well in discriminating between healthy and glaucomatous eyes and correlate well with the location of visual field deficit [116–121]. Using ONH parameters, Moorfields Regression

Analysis (MRA) was developed to improve the diagnostic accuracy of the HRT. MRA uses optic disc and neuroretinal rim areas both globally and in six sectors and compares it with a normative database adjusted for optic disc size and age [122, 123]. MRA achieved higher sensitivity and specificity for identifying glaucomatous optic discs than any other imaging technology available at that time [122]. HRT was also shown to allow the detection of structural changes before the appearance of changes in perimetry [10, 124–126].

The primary progression analysis method provided by HRT is the Topographic Change Analysis (TCA). This method calculates a probability map based on locations changing beyond the measurement variability [127]. In a longitudinal study, HRT documented a higher rate of progression than the rate observed by perimetry [127], but as in most longitudinal studies, it is not clear if these eyes reflect actual disease progression.

HRT measurements showed high reproducibility [128] that was further improved when multiple scans were averaged, which lead to the practice of combining data from three scans [129].

Conclusion

Early detection and monitoring of glaucoma progression are crucial to preserve long-term functional vision. The emergence of accurate, reproducible, and sensitive imaging modalities that complement the clinical judgment has revolutionized glaucoma practice worldwide. Among several imaging that were used over the years, OCT has become the leading tool in glaucoma evaluation. The micron scale optical sampling provided by the device is clinically useful for several subspecialty in ophthalmology increasing its attraction. New and appealing OCT-based technologies and application emerge, such as the OCTA and the deployment of AI. The next decade will likely experience significant developments, making glaucoma practice a dynamic, exciting, and fulfilling one.

References

- Helmholtz J. Beschreibung eines Augenspiegels zur Untersuchung der Netzhaut in lebenden Augi. Berlin: A Forstner; 1851.
- Graefe AV. Ueber die wirkung der Iridectomie bei Glaucom. Arch Ophthalmol. 1857;3:456.
- Schnabel I. Die Entwicklungsgeschichte der glaukomatösen Exkavation. Z Augenheilkd. 1905;14:1.
- Elliot R. Treatise on glaucoma. London: Henry Fraude and Hodder & Stroughton LTD; 1922. p. 195.
- Quigley HA, Addicks EM, Green WR. Optic nerve damage in human glaucoma. III. Quantitative correlation of nerve fiber loss and visual field defect in glaucoma, ischemic neuropathy, papilledema, and toxic neuropathy. Arch Ophthalmol. 1982;100(1):135–46.
- Quigley HA, Miller NR, George T. Clinical evaluation of nerve fiber layer atrophy as an indicator of glaucomatous optic nerve damage. Arch Ophthalmol. 1980;98(9):1564–71.
- Lucy KA, Wollstein G. Structural and functional evaluations for the early detection of glaucoma. Expert Rev Ophthalmol. 2016;11(5):367–76.
- Kuang TM, Zhang C, Zangwill LM, Weinreb RN, Medeiros FA. Estimating lead time gained by optical coherence tomography in detecting glaucoma before development of visual field defects. Ophthalmology. 2015;122(10):2002–9.
- Wollstein G, Schuman JS, Price LL, Aydin A, Stark PC, Hertzmark E, et al. Optical coherence tomography longitudinal evaluation of retinal nerve fiber layer thickness in glaucoma. Arch Ophthalmol. 2005;123(4):464–70.
- Weinreb RN, Zangwill LM, Jain S, Becerra LM, Dirkes K, Piltz-Seymour JR, et al. Predicting the onset of glaucoma: the confocal scanning laser ophthalmoscopy ancillary study to the Ocular Hypertension Treatment Study. Ophthalmology. 2010;117(9):1674–83.
- Reus NJ, Lemij HG. Relationships between standard automated perimetry, HRT confocal scanning laser ophthalmoscopy, and GDx VCC scanning laser polarimetry. Invest Ophthalmol Vis Sci. 2005;46(11):4182–8.
- Jonas JB, Aung T, Bourne RR, Bron AM, Ritch R, Panda-Jonas S. Glaucoma. Lancet (London, England). 2017;390(10108):2183–93.
- Gandhi M, Dubey S. Evaluation of the optic nerve head in glaucoma. J Curr Glaucoma Pract. 2013;7(3):106–14.
- Lichter PR. Variability of expert observers in evaluating the optic disc. Trans Am Ophthalmol Soc. 1976;74:532–72.
- Jackman WT, Webster J. On photographing the retina of the living human eye. Phila Photogr. 1886;23:340–1.
- Parsons H. The photography of the fundus oculi. Nature. 1906;74:104.
- Van Cader T. History of ophthalmic photography. J Ophthal Photogr. 1978;1(1):7.
- Spaeth GL, Reddy SC. Imaging of the optic disk in caring for patients with glaucoma: ophthalmoscopy and photography remain the gold standard. Surv Ophthalmol. 2014;59(4):454–8.
- Tielsch JM, Katz J, Quigley HA, Miller NR, Sommer A. Intraobserver and interobserver agreement in measurement of optic disc characteristics. Ophthalmology. 1988;95(3):350–6.
- Gaasterland DE, Blackwell B, Dally LG, Caprioli J, Katz LJ, Ederer F. The advanced glaucoma intervention study (AGIS): 10. Variability among academic glaucoma subspecialists in assessing optic disc notching. Trans Am Ophthalmol Soc. 2001;99:177–84.
- Reus NJ, Lemij HG, Garway-Heath DF, Airaksinen PJ, Anton A, Bron AM, et al. Clinical assessment of stereoscopic optic disc photographs for glaucoma: the European Optic Disc Assessment Trial. Ophthalmology. 2010;117(4):717–23.
- Ervin AM, Boland MV, Myrowitz EH, Prince J, Hawkins B, Vollenweider D, Ward D, et al. Screening for glaucoma: comparative effectiveness. AHRQ Comparative Effectiveness Review. 12:EHC037-EF. Rockville: Agency for Healthcare Research and Quality (US); 2012.
- Budenz DL, Anderson DR, Feuer WJ, Beiser JA, Schiffman J, Parrish RK, Piltz-Seymour JR, et al. Detection and prognostic significance of optic disc hemorrhages during the Ocular Hypertension Treatment Study. Ophthalmology. 2006;113(12):2137–43.
- Panwar N, Huang P, Lee J, Keane PA, Chuan TS, Richhariya A, et al. Fundus photography in the 21st century – a review of recent technological advances and their implications for worldwide healthcare. Telemed E-Health. 2016;22(3):198–208.
- Myers JS, Fudenberg SJ, Lee D. Evolution of optic nerve photography for glaucoma screening: a review. Clin Exp Ophthalmol. 2018;46(2):169–76.
- Zheng C, Johnson TV, Garg A, Boland MV. Artificial intelligence in glaucoma. Curr Opin Ophthalmol. 2019;30(2):97–103.
- Ting DSW, Cheung CY, Lim G, Tan GSW, Quang ND, Gan A, et al. Development and validation of a deep learning system for diabetic retinopathy and related eye diseases using retinal images from multiethnic populations with diabetes. JAMA. 2017;318(22):2211–23.
- Li Z, He Y, Keel S, Meng W, Chang RT, He M. Efficacy of a deep learning system for detecting glaucomatous optic neuropathy based on color fundus photographs. Ophthalmology. 2018;125(8):1199–206.
- Huang D, Swanson EA, Lin CP, Schuman JS, Stinson WG, Chang W, et al. Optical coherence tomography. Science (New York, NY). 1991;254(5035):1178–81.
- Hougaard JL, Heijl A, Bengtsson B. Glaucoma detection by stratus OCT. J Glaucoma. 2007;16(3):302–6.
- Parikh RS, Parikh S, Sekhar GC, Kumar RS, Prabakaran S, Babu JG, et al. Diagnostic capability of

- optical coherence tomography (Stratus OCT 3) in early glaucoma. *Ophthalmology*. 2007;114(12):2238–43.
32. Nouri-Mahdavi K, Nikkhou K, Hoffman DC, Law SK, Caprioli J. Detection of early glaucoma with optical coherence tomography (Stratus OCT). *J Glaucoma*. 2008;17(3):183–8.
 33. Medeiros FA, Zangwill LM, Alencar LM, Bowd C, Sample PA, Susanna R Jr, et al. Detection of glaucoma progression with stratus OCT retinal nerve fiber layer, optic nerve head, and macular thickness measurements. *Invest Ophthalmol Vis Sci*. 2009;50(12):5741–8.
 34. Dong ZM, Wollstein G, Schuman JS. Clinical utility of optical coherence tomography in glaucoma. *Invest Ophthalmol Vis Sci*. 2016;57(9):OCT556–67.
 35. Sung KR, Kim JS, Wollstein G, Folio L, Kook MS, Schuman JS. Imaging of the retinal nerve fiber layer with spectral domain optical coherence tomography for glaucoma diagnosis. *Br J Ophthalmol*. 2011;95(7):909–14.
 36. Leung CK, Cheung CY, Weinreb RN, Qiu Q, Liu S, Li H, et al. Retinal nerve fiber layer imaging with spectral-domain optical coherence tomography: a variability and diagnostic performance study. *Ophthalmology*. 2009;116(7):1257–63, 63.e1–2.
 37. Kim JS, Ishikawa H, Sung KR, Xu J, Wollstein G, Bilonick RA, et al. Retinal nerve fibre layer thickness measurement reproducibility improved with spectral domain optical coherence tomography. *Br J Ophthalmol*. 2009;93(8):1057–63.
 38. Mwanza JC, Oakley JD, Budenz DL, Anderson DR. Ability of cirrus HD-OCT optic nerve head parameters to discriminate normal from glaucomatous eyes. *Ophthalmology*. 2011;118(2):241–8.e1.
 39. Leung CK, Chiu V, Weinreb RN, Liu S, Ye C, Yu M, et al. Evaluation of retinal nerve fiber layer progression in glaucoma: a comparison between spectral-domain and time-domain optical coherence tomography. *Ophthalmology*. 2011;118(8):1558–62.
 40. Schuman JS. Spectral domain optical coherence tomography for glaucoma (an AOS thesis). *Trans Am Ophthalmol Soc*. 2008;106:426–58.
 41. Wojtkowski M, Srinivasan V, Fujimoto JG, Ko T, Schuman JS, Kowalczyk A, et al. Three-dimensional retinal imaging with high-speed ultrahigh-resolution optical coherence tomography. *Ophthalmology*. 2005;112(10):1734–46.
 42. Kostanyan T, Wollstein G, Schuman JS. New developments in optical coherence tomography. *Curr Opin Ophthalmol*. 2015;26(2):110–5.
 43. Potsaid B, Baumann B, Huang D, Barry S, Cable AE, Schuman JS, et al. Ultrahigh speed 1050nm swept source/Fourier domain OCT retinal and anterior segment imaging at 100,000 to 400,000 axial scans per second. *Opt Express*. 2010;18(19):20029–48.
 44. Srinivasan VJ, Adler DC, Chen Y, Gorczynska I, Huber R, Duker JS, et al. Ultrahigh-speed optical coherence tomography for three-dimensional and en face imaging of the retina and optic nerve head. *Invest Ophthalmol Vis Sci*. 2008;49(11):5103–10.
 45. Fallon M, Valero O, Pazos M, Anton A. Diagnostic accuracy of imaging devices in glaucoma: a meta-analysis. *Surv Ophthalmol*. 2017;62(4):446–61.
 46. Rao HL, Zangwill LM, Weinreb RN, Sample PA, Alencar LM, Medeiros FA. Comparison of different spectral domain optical coherence tomography scanning areas for glaucoma diagnosis. *Ophthalmology*. 2010;117(9):1692–9.
 47. Oddone F, Lucenteforte E, Michelessi M, Rizzo S, Donati S, Parravano M, et al. Macular versus retinal nerve fiber layer parameters for diagnosing manifest glaucoma: a systematic review of diagnostic accuracy studies. *Ophthalmology*. 2016;123(5):939–49.
 48. Bussell II, Wollstein G, Schuman JS. OCT for glaucoma diagnosis, screening and detection of glaucoma progression. *Br J Ophthalmol*. 2014;98(Suppl 2):ii15–9.
 49. Leite MT, Zangwill LM, Weinreb RN, Rao HL, Alencar LM, Sample PA, et al. Effect of disease severity on the performance of Cirrus spectral-domain OCT for glaucoma diagnosis. *Invest Ophthalmol Vis Sci*. 2010;51(8):4104–9.
 50. Bengtsson B, Andersson S, Heijl A. Performance of time-domain and spectral-domain Optical Coherence Tomography for glaucoma screening. *Acta Ophthalmol*. 2012;90(4):310–5.
 51. Curcio CA, Allen KA. Topography of ganglion cells in human retina. *J Comp Neurol*. 1990;300(1):5–25.
 52. Jeong JS, Kang MG, Kim CY, Kim NR. Pattern of macular ganglion cell-inner plexiform layer defect generated by spectral-domain OCT in glaucoma patients and normal subjects. *J Glaucoma*. 2015;24(8):583–90.
 53. Tan O, Chopra V, Lu AT, Schuman JS, Ishikawa H, Wollstein G, et al. Detection of macular ganglion cell loss in glaucoma by Fourier-domain optical coherence tomography. *Ophthalmology*. 2009;116(12):2305–14.
 54. Zangalli CS, Ahmed OM, Waisbourd M, Ali MH, Cvintal V, Affel E, et al. Segmental analysis of macular layers in patients with unilateral primary open-angle glaucoma. *J Glaucoma*. 2016;25(4):e401–7.
 55. Lisboa R, Paranhos A Jr, Weinreb RN, Zangwill LM, Leite MT, Medeiros FA. Comparison of different spectral domain OCT scanning protocols for diagnosing preperimetric glaucoma. *Invest Ophthalmol Vis Sci*. 2013;54(5):3417–25.
 56. Pollet-Villard F, Chiquet C, Romanet JP, Noel C, Aptel F. Structure-function relationships with spectral-domain optical coherence tomography retinal nerve fiber layer and optic nerve head measurements. *Invest Ophthalmol Vis Sci*. 2014;55(5):2953–62.
 57. Fan KC, Tsikata E, Khoueir Z, Simavli H, Guo R, de Luna RA, et al. Enhanced diagnostic capability for glaucoma of 3-dimensional versus 2-dimensional neuroretinal rim parameters using spectral domain optical coherence tomography. *J Glaucoma*. 2017;26(5):450–8.

58. Sung KR, Na JH, Lee Y. Glaucoma diagnostic capabilities of optic nerve head parameters as determined by cirrus HD optical coherence tomography. *J Glaucoma*. 2012;21(7):498–504.
59. Hood DC, De Cuir N, Blumberg DM, Liebmann JM, Jarukasetphon R, Ritch R, et al. A single wide-field OCT protocol can provide compelling information for the diagnosis of early glaucoma. *Transl Vis Sci Technol*. 2016;5(6):4.
60. Lee WJ, Na KI, Kim YK, Jeoung JW, Park KH. Diagnostic ability of wide-field retinal nerve fiber layer maps using swept-source optical coherence tomography for detection of preperimetric and early perimetric glaucoma. *J Glaucoma*. 2017;26(6):577–85.
61. Lee WJ, Kim TJ, Kim YK, Jeoung JW, Park KH. Serial combined wide-field optical coherence tomography maps for detection of early glaucomatous structural progression. *JAMA Ophthalmol*. 2018;136(10):1121–7.
62. Lee WJ, Oh S, Kim YK, Jeoung JW, Park KH. Comparison of glaucoma-diagnostic ability between wide-field swept-source OCT retinal nerve fiber layer maps and spectral-domain OCT. *Eye*. 2018;32(9):1483–92.
63. Balyen L, Peto T. Promising artificial intelligence-machine learning-deep learning algorithms in ophthalmology. *Asia-Pac J Ophthalmol*. 2019;8(3):264–72.
64. Grewal PS, Oloumi F, Rubin U, Tennant MTS. Deep learning in ophthalmology: a review. *Can J Ophthalmol*. 2018;53(4):309–13.
65. Wu Z, Medeiros FA. Comparison of visual field point-wise event-based and global trend-based analysis for detecting glaucomatous progression. *Transl Vis Sci Technol*. 2018;7(4):20.
66. Tatham AJ, Medeiros FA. Detecting structural progression in glaucoma with optical coherence tomography. *Ophthalmology*. 2017;124(12s):S57–65.
67. Hammel N, Belghith A, Weinreb RN, Medeiros FA, Mendoza N, Zangwill LM. Comparing the rates of retinal nerve fiber layer and ganglion cell-inner plexiform layer loss in healthy eyes and in glaucoma eyes. *Am J Ophthalmol*. 2017;178:38–50.
68. Shin JW, Sung KR, Lee GC, Durbin MK, Cheng D. Ganglion cell-inner plexiform layer change detected by optical coherence tomography indicates progression in advanced glaucoma. *Ophthalmology*. 2017;124(10):1466–74.
69. Zhang X, Loewen N, Tan O, Greenfield DS, Schuman JS, Varma R, et al. Predicting development of glaucomatous visual field conversion using baseline Fourier-domain optical coherence tomography. *Am J Ophthalmol*. 2016;163:29–37.
70. Leung CK, Yu M, Weinreb RN, Ye C, Liu S, Lai G, et al. Retinal nerve fiber layer imaging with spectral-domain optical coherence tomography: a prospective analysis of age-related loss. *Ophthalmology*. 2012;119(4):731–7.
71. Zhang X, Francis BA, Dastiridou A, Chopra V, Tan O, Varma R, et al. Longitudinal and cross-sectional analyses of age effects on retinal nerve fiber layer and ganglion cell complex thickness by Fourier-domain OCT. *Transl Vis Sci Technol*. 2016;5(2):1.
72. Mwanza JC, Chang RT, Budenz DL, Durbin MK, Gendy MG, Shi W, et al. Reproducibility of peripapillary retinal nerve fiber layer thickness and optic nerve head parameters measured with cirrus HD-OCT in glaucomatous eyes. *Invest Ophthalmol Vis Sci*. 2010;51(11):5724–30.
73. Kim KE, Yoo BW, Jeoung JW, Park KH. Long-term reproducibility of macular ganglion cell analysis in clinically stable glaucoma patients. *Invest Ophthalmol Vis Sci*. 2015;56(8):4857–64.
74. Wang RK, Jacques SL, Ma Z, Hurst S, Hanson SR, Gruber A. Three dimensional optical angiography. *Opt Express*. 2007;15(7):4083–97.
75. Hope-Ross M, Yannuzzi LA, Gragoudas ES, Guyer DR, Slakter JS, Sorenson JA, et al. Adverse reactions due to indocyanine green. *Ophthalmology*. 1994;101(3):529–33.
76. Lopez-Saez MP, Ordoqui E, Tornero P, Baeza A, Sainza T, Zubeldia JM, et al. Fluorescein-induced allergic reaction. *Ann Allergy Asthma Immunol*. 1998;81(5):428–30.
77. Liu L, Jia Y, Takusagawa HL, Pechauer AD, Edmunds B, Lombardi L, et al. Optical coherence tomography angiography of the peripapillary retina in glaucoma. *JAMA Ophthalmol*. 2015;133(9):1045–52.
78. Yarmohammadi A, Zangwill LM, Diniz-Filho A, Suh MH, Manalastas PI, Fatehee N, et al. Optical coherence tomography angiography vessel density in healthy, glaucoma suspect, and glaucoma eyes. *Invest Ophthalmol Vis Sci*. 2016;57(9):Oct451–9.
79. Rao HL, Kadambi SV, Weinreb RN, Puttaiah NK, Pradhan ZS, Rao DAS, et al. Diagnostic ability of peripapillary vessel density measurements of optical coherence tomography angiography in primary open-angle and angle-closure glaucoma. *Br J Ophthalmol*. 2017;101(8):1066–70.
80. Geyman LS, Garg RA, Suwan Y, Trivedi V, Krawitz BD, Mo S, et al. Peripapillary perfused capillary density in primary open-angle glaucoma across disease stage: an optical coherence tomography angiography study. *Br J Ophthalmol*. 2017;101(9):1261–8.
81. Chihara E, Dimitrova G, Amano H, Chihara T. Discriminatory power of superficial vessel density and prelaminar vascular flow index in eyes with glaucoma and ocular hypertension and normal eyes. *Invest Ophthalmol Vis Sci*. 2017;58(1):690–7.
82. Yarmohammadi A, Zangwill LM, Manalastas PIC, Fuller NJ, Diniz-Filho A, Saunders LJ, et al. Peripapillary and macular vessel density in patients with primary open-angle glaucoma and unilateral visual field loss. *Ophthalmology*. 2018;125(4):578–87.
83. Van Melkebeke L, Barbosa-Breda J, Huygens M, Stalmans I. Optical coherence tomography angiography in glaucoma: a review. *Ophthalmic Res*. 2018;60(3):139–51.

84. Mwanza JC, Budenz DL. New developments in optical coherence tomography imaging for glaucoma. *Curr Opin Ophthalmol*. 2018;29(2):121–9.
85. Hou H, Moghimi S, Zangwill LM, Shoji T, Ghahari E, Manalastas PIC, et al. Inter-eye asymmetry of optical coherence tomography angiography vessel density in bilateral glaucoma, glaucoma suspect, and healthy eyes. *Am J Ophthalmol*. 2018;190:69–77.
86. Chen CL, Bojikian KD, Wen JC, Zhang Q, Xin C, Mudumbai RC, et al. Peripapillary retinal nerve fiber layer vascular microcirculation in eyes with glaucoma and single-hemifield visual field loss. *JAMA Ophthalmol*. 2017;135(5):461–8.
87. Penteado RC, Zangwill LM, Daga FB, Saunders LJ, Manalastas PIC, Shoji T, et al. Optical coherence tomography angiography macular vascular density measurements and the central 10-2 visual field in glaucoma. *J Glaucoma*. 2018;27(6):481–9.
88. Yarmohammadi A, Zangwill LM, Diniz-Filho A, Suh MH, Yousefi S, Saunders LJ, et al. Relationship between optical coherence tomography angiography vessel density and severity of visual field loss in glaucoma. *Ophthalmology*. 2016;123(12):2498–508.
89. Pradhan ZS, Dixit S, Sreenivasiah S, Rao HL, Venugopal JP, Devi S, et al. A sectoral analysis of vessel density measurements in perimetrically intact regions of glaucomatous eyes: an optical coherence tomography angiography study. *J Glaucoma*. 2018;27(6):525–31.
90. Sakaguchi K, Higashide T, Udagawa S, Ohkubo S, Sugiyama K. Comparison of sectoral structure-function relationships in glaucoma: vessel density versus thickness in the peripapillary retinal nerve fiber layer. *Invest Ophthalmol Vis Sci*. 2017;58(12):5251–62.
91. Bojikian KD, Chen PP, Wen JC. Optical coherence tomography angiography in glaucoma. *Curr Opin Ophthalmol*. 2019;30(2):110–6.
92. Moghimi S, Bowd C, Zangwill LM, Penteado RC, Hasenstab K, Hou H, et al. Measurement floors and dynamic ranges of OCT and OCT angiography in glaucoma. *Ophthalmology*. 2019;126(7):980–8.
93. Suwan Y, Fard MA, Geyman LS, Tantraworasin A, Chui TY, Rosen RB, et al. Association of myopia with peripapillary perfused capillary density in patients with glaucoma: an optical coherence tomography angiography study. *JAMA Ophthalmol*. 2018;136(5):507–13.
94. Shin JW, Kwon J, Lee J, Kook MS. Relationship between vessel density and visual field sensitivity in glaucomatous eyes with high myopia. *Br J Ophthalmol*. 2019;103:585–591.
95. Lombardo M, Serrao S, Devaney N, Parravano M, Lombardo G. Adaptive optics technology for high-resolution retinal imaging. *Sensors (Basel, Switzerland)*. 2012;13(1):334–66.
96. Dreher AW, Bille JF, Weinreb RN. Active optical depth resolution improvement of the laser tomographic scanner. *Appl Opt*. 1989;28(4):804–8.
97. Dong ZM, Wollstein G, Wang B, Schuman JS. Adaptive optics optical coherence tomography in glaucoma. *Prog Retin Eye Res*. 2017;57:76–88.
98. Jonnal RS, Kocaoglu OP, Zawadzki RJ, Liu Z, Miller DT, Werner JS. A review of adaptive optics optical coherence tomography: technical advances, scientific applications, and the future. *Invest Ophthalmol Vis Sci*. 2016;57(9):Oct51–68.
99. Liu Z, Kurokawa K, Zhang F, Lee JJ, Miller DT. Imaging and quantifying ganglion cells and other transparent neurons in the living human retina. *Proc Natl Acad Sci U S A*. 2017;114(48):12803–8.
100. Wang B, Lucy KA, Schuman JS, Sigal IA, Bilonick RA, Lu C, et al. Tortuous pore path through the glaucomatous lamina cribrosa. *Sci Rep*. 2018;8(1):7281.
101. Nadler Z, Wang B, Schuman JS, Ferguson RD, Patel A, Hammer DX, et al. In vivo three-dimensional characterization of the healthy human lamina cribrosa with adaptive optics spectral-domain optical coherence tomography. *Invest Ophthalmol Vis Sci*. 2014;55(10):6459–66.
102. Ivers KM, Sredar N, Patel NB, Rajagopalan L, Queener HM, Twa MD, et al. In vivo changes in lamina cribrosa microarchitecture and optic nerve head structure in early experimental glaucoma. *PLoS One*. 2015;10(7):e0134223.
103. Kim TW, Kagemann L, Girard MJ, Strouthidis NG, Sung KR, Leung CK, et al. Imaging of the lamina cribrosa in glaucoma: perspectives of pathogenesis and clinical applications. *Curr Eye Res*. 2013;38(9):903–9.
104. de Boer JF, Hitzengerger CK, Yasuno Y. Polarization sensitive optical coherence tomography – a review [Invited]. *Biomed Opt Express*. 2017;8(3):1838–73.
105. Dwelle J, Liu S, Wang B, McElroy A, Ho D, Markey MK, et al. Thickness, phase retardation, birefringence, and reflectance of the retinal nerve fiber layer in normal and glaucomatous non-human primates. *Invest Ophthalmol Vis Sci*. 2012;53(8):4380–95.
106. Liu S, Wang B, Yin B, Milner TE, Markey MK, McKinnon SJ, et al. Retinal nerve fiber layer reflectance for early glaucoma diagnosis. *J Glaucoma*. 2014;23(1):e45–52.
107. Gardiner SK, Demirel S, Reynaud J, Fortune B. Changes in retinal nerve fiber layer reflectance intensity as a predictor of functional progression in glaucoma. *Invest Ophthalmol Vis Sci*. 2016;57(3):1221–7.
108. Huang XR, Zhou Y, Kong W, Knighton RW. Reflectance decreases before thickness changes in the retinal nerve fiber layer in glaucomatous retinas. *Invest Ophthalmol Vis Sci*. 2011;52(9):6737–42.
109. Leitgeb RA, Werkmeister RM, Blatter C, Schmetterer L. Doppler optical coherence tomography. *Prog Retin Eye Res*. 2014;41:26–43.
110. Sehi M, Goharian I, Konduru R, Tan O, Srinivas S, Sadda SR, et al. Retinal blood flow in glaucomatous

- eyes with single-hemifield damage. *Ophthalmology*. 2014;121(3):750–8.
111. Kirby MA, Pelivanov I, Song S, Ambrozinski L, Yoon SJ, Gao L, et al. Optical coherence elastography in ophthalmology. *J Biomed Opt*. 2017;22(12):1–28.
 112. Singh M, Li J, Han Z, Raghunathan R, Nair A, Wu C, et al. Assessing the effects of riboflavin/UV-A crosslinking on porcine corneal mechanical anisotropy with optical coherence elastography. *Biomed Opt Express*. 2017;8(1):349–66.
 113. Torricelli AA, Bechara SJ, Wilson SE. Screening of refractive surgery candidates for LASIK and PRK. *Cornea*. 2014;33(10):1051–5.
 114. Moon S, Choi ES. VCSEL-based swept source for low-cost optical coherence tomography. *Biomed Opt Express*. 2017;8(2):1110–21.
 115. Lu CD, Waheed NK, Witkin A, Bauman CR, Liu JJ, Potsaid B, et al. Microscope-integrated intraoperative ultrahigh-speed swept-source optical coherence tomography for widefield retinal and anterior segment imaging. *Ophthalmic Surg Lasers Imaging Retina*. 2018;49(2):94–102.
 116. Uchida H, Brigatti L, Caprioli J. Detection of structural damage from glaucoma with confocal laser image analysis. *Invest Ophthalmol Vis Sci*. 1996;37(12):2393–401.
 117. Zangwill LM, van Horn S, Lima MD, Sample PA, Weinreb RN. Optic nerve head topography in ocular hypertensive eyes using confocal scanning laser ophthalmoscopy. *Am J Ophthalmol*. 1996;122(4):520–5.
 118. Iester M, De Ferrari R, Zanini M. Topographic analysis to discriminate glaucomatous from normal optic nerve heads with a confocal scanning laser: new optic disk analysis without any observer input. *Surv Ophthalmol*. 1999;44:S33–40.
 119. Iester M, Mikelberg FS, Courtright P, Drance SM. Correlation between the visual field indices and Heidelberg retina tomograph parameters. *J Glaucoma*. 1997;6(2):78–82.
 120. Gulati V, Agarwal HC, Sihota R, Saxena R. Correlation analysis of visual field thresholds and scanning laser ophthalmoscopic optic nerve head measurements in glaucoma. *Ophthalmic Physiol Opt*. 2003;23(3):233–42.
 121. Ferreras A, Pablo LE, Larrosa JM, Polo V, Pajarin AB, Honrubia FM. Discriminating between normal and glaucoma-damaged eyes with the Heidelberg retina tomograph 3. *Ophthalmology*. 2008;115(5):775–81.
 122. Wollstein G, Garway-Heath DF, Hitchings RA. Identification of early glaucoma cases with the scanning laser ophthalmoscope. *Ophthalmology*. 1998;105(8):1557–63.
 123. Miglior S, Guareschi M, Albe E, Gomasasca S, Vavassori M, Orzalesi N. Detection of glaucomatous visual field changes using the Moorfields regression analysis of the Heidelberg retina tomograph. *Am J Ophthalmol*. 2003;136(1):26–33.
 124. Kamal DS, Viswanathan AC, Garway-Heath DF, Hitchings RA, Poinosawmy D, Bunce C. Detection of optic disc change with the Heidelberg retina tomograph before confirmed visual field change in ocular hypertensives converting to early glaucoma. *Br J Ophthalmol*. 1999;83(3):290–4.
 125. Zangwill LM, Weinreb RN, Beiser JA, Berry CC, Cioffi GA, Coleman AL, et al. Baseline topographic optic disc measurements are associated with the development of primary open-angle glaucoma: the confocal scanning laser ophthalmoscopy ancillary study to the ocular hypertension treatment study. *Arch Ophthalmol*. 2005;123(9):1188–97.
 126. Alencar LM, Bowd C, Weinreb RN, Zangwill LM, Sample PA, Medeiros FA. Comparison of HRT-3 glaucoma probability score and subjective stereophotograph assessment for prediction of progression in glaucoma. *Invest Ophthalmol Vis Sci*. 2008;49(5):1898–906.
 127. Chauhan BC, Blanchard JW, Hamilton DC, LeBlanc RP. Technique for detecting serial topographic changes in the optic disc and peripapillary retina using scanning laser tomography. *Invest Ophthalmol Vis Sci*. 2000;41(3):775–82.
 128. DeLeon Ortega JE, Sakata LM, Kakati B, McGwin G Jr, Monheit BE, Arthur SN, et al. Effect of glaucomatous damage on repeatability of confocal scanning laser ophthalmoscope, scanning laser polarimetry, and optical coherence tomography. *Invest Ophthalmol Vis Sci*. 2007;48(3):1156–63.
 129. Weinreb RN, Lusky M, Bartsch DU, Morsman D. Effect of repetitive imaging on topographic measurements of the optic nerve head. *Arch Ophthalmol*. 1993;111(5):636–8.

reproduced in whole
or in part, nor passed
to any third party.